Superlattices and Microstructures, Vol. 25, No. 3, 1999
Article No. spmi.1998.0601
Available online at http://www.idealibrary.com on IDEAL

Feasibility study of the quantum XOR gate based on coupled asymmetric semiconductor quantum dots

A. BALANDIN, K. L. WANG
Device Research Laboratory, Electrical Engineering Department, University of California – Los Angeles, Los Angeles, CA 90095-1594, U.S.A.

(Received 8 September 1998)

We propose an implementation of the quantum XOR (controlled-NOT) gate on the basis of coupled *asymmetric* quantum dots. Results of our numerical simulations show that the coupling constant of the dipole–dipole interaction and the probability of spontaneous emission can be tuned over a wide range by a proper choice of the potential profile, material parameters, and distances between the dots. We argue that the use of the asymmetric potential profile provides better conditions for having the Ising-type interaction between the dots than earlier proposed schemes based on regular symmetric quantum dots biased with an electric field. Our system gives better resolution of different quantum states, avoids any undesirable time evolution of these states, and can be driven with a femtosecond laser. The qubit manipulation and time coherency requirements are also discussed.

Key words: quantum computing, asymmetric quantum dot, dipole interaction.

1. Introduction

Development of quantum computation schemes has led to many proposals of potentially realizable quantum computers based on various physical systems. Among the most well-known are quantum computers that utilize laser-trapped ions [1], nuclear magnetic resonance (NMR) systems [2], all-optical logic gates [3], Josephson junctions [4] and semiconductor nanostructures [5]. Successful experimental demonstrations of one and two qubit computers were reported for laser-trapped ion systems [6] and NMR systems [7]. The progress in theoretical and experimental development of quantum logic gates on the basis of semiconductor nanostructures has been far short of these systems. This is primarily due to the difficulties in fabrication of high quality quantum dot arrays with a number of almost identical dots, and the decoherence problem [8] which is inherently more severe for solid state systems [9]. On the other hand, if these problems are overcome, the quantum computer based on semiconductor quantum dots offers an attractive alternative to other physical implementations due to its compactness, robustness, and the larger number of qubits which can be realized [10]. Some of these advantages were discussed previously in the context of nanoelectronic architecture for Boolean logic gates [11, 12]. Another important advantage of the quantum dot implementation is that further development can make use of well-developed conventional semiconductor technology [13].

In this paper we propose a solid state implementation of the quantum XOR gate (also called controlled-NOT gate) based on coupled *asymmetrical quantum dots*. We present a feasibility study of this implementation which

0749–6036/99/030509 + 10 $30.00/0

includes calculation of the coupling constants and the decoherence time. The rest of the paper is organized as follows. The gate structure and its operation are outlined in Sections 2 and 3, respectively. In Section 4, we present numerically calculated charge density distributions and coupling constants in asymmetric quantum dots. These results are followed by a discussion and comparison with other implementations. Evaluation of the decoherence processes associated with our structure is presented in Section 5. Conclusions are given in Section 6.

2. Gate structure

A classical controlled-NOT gate is a two-bit operator, in which the first bit is the control and the second bit is the target. Its operation or the truth table can be written as follows.

$$CN := |00\rangle\langle 00| + |01\rangle\langle 01| + |10\rangle\langle 11| + |11\rangle\langle 10|. \tag{1}$$

Here, if the control bit is in the state $|0\rangle$, the target bit does not change its value after the action of the gate, but if the control bit is in the state $|1\rangle$, the target changes its value after the action of the gate (the last two terms of eqn (1)). Since this gate is logically and physically reversible, it is in principle capable of quantum computing [5, 14]. In order to do this, the gate must act on superpositions of bits (qubits) and coherently transform them in accordance with the rule $a|00\rangle + b|11\rangle \rightarrow a|00\rangle + b|10\rangle$. Here each member of the quantum superposition transforms according to the classical rule for the gate. Such a gate is conventionally called the quantum XOR gate.

We propose an implementation of the XOR gate with the computational basis states, $\{|0\rangle,\ |1\rangle\}$ formed by the ground and the first excited states of two semiconductor single-electron quantum dots. Application of a $\pi/2$ pulse or some other fractions of a π pulse will place the gate into a coherent superposition of two states $|0\rangle$ and $|1\rangle$ thus allowing for initial preparation of a qubit. Owing to the asymmetry of the confining potentials of the two dots and their corresponding uneven charge distributions, the dipole moments p_{ground} and p_{excited} are induced in the ground and excited states, $|0\rangle$ and $|1\rangle$, respectively (since the dipoles are parallel, we do not use the vector notation). These dipoles are defined as

$$p_i = \int_{-W/2-\Delta}^{W/2+\Delta} \Psi_i z \Psi_i^* \, dz, \tag{2}$$

where z is the axis along the growth direction (see inset to Fig. 1), W is the size of the dot along the z-axis, Ψ is the electron wavefunction, Δ is the maximum wavefunction barrier penetration depth, and the index i denotes either the *ground* or *excited* states of the same dot.

The conditional dynamics of the two-dot structure is achieved via dipole–dipole interaction between two neighboring dots as in Ref. [5]. The first quantum dot with resonant energy $\hbar\omega_c$ (the transition energy between states $|1\rangle$ and $|0\rangle$) acts as the control qubit while the second dot with resonant energy $\hbar\omega_t$ acts as the target qubit. The gate is driven optically by application of a proper train of π/N pulses (N is some positive number) which allow one to prepare the qubits, perform Hadamard transfers, and other operations needed for quantum computing [15].

The asymmetry of the potential well has an effect similar to that of applying an electric field [5] while allowing for more degrees of freedom. Control of the potential profile provides better tuning capabilities for dipole moments, so that dipoles of the computational basis states can be made exactly equal in their absolute values while opposite in their signs

$$p_{\text{ground}} = -p_{\text{excited}}. \tag{3}$$

The latter is required to have a desirable Ising-type coupling interaction between the dipoles of the two dots. Moreover, we will argue that it is extremely difficult if not impossible to meet the requirement of eqn (3) in symmetric quantum dots for realistic values of material parameters and a biasing electric field. In principle,

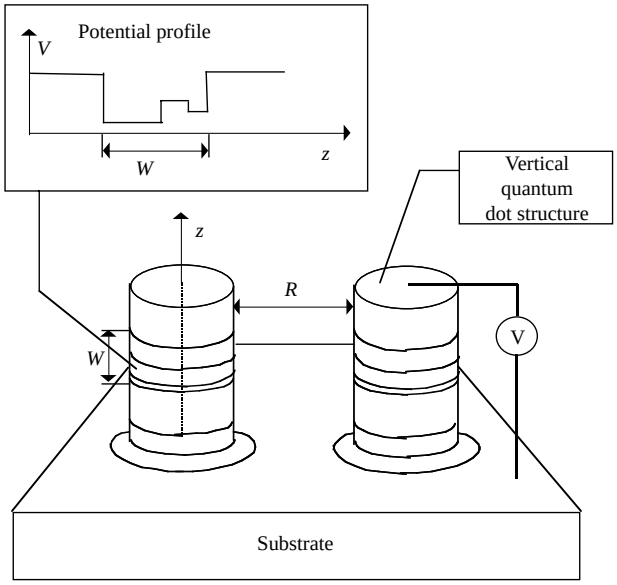

Fig. 1. Structure of the single-electron asymmetric quantum dots. Inset shows an example of the potential profile of a quantum dot along the growth direction.

conditional quantum dynamics with the resonant frequency of one dot depending on the neighboring dot's state can be built from any such dots brought close together in the Coulomb interaction range [10, 16]. But it turns out that in order to have a better resolution of different quantum states and to avoid any undesirable evolution of these states, it is better to construct a system which can be described by an Ising-type interaction [14].

The proposed structure can be implemented using state-of-the-art technology of quantum dots which can be fabricated in a vertical configuration [17, 18]. Specifically, we will consider an $Al_xGa_{1-x}As/GaAs$ vertical quantum dot structure containing a tunable number of electrons. Experimental demonstrations of such structures containing from zero to 50 electrons were reported in Refs [19, 20]. By controlling the potential profile of the dots along the growth direction, one can adjust the system in such a way that the condition of eqn (3) holds true [21]. An example of a prototype structure with the desirable potential profile is shown in Fig. 1. The gate bias which is required for localization of one electron in the dot structure is of the order of $|V_G| = 0.1$–0.7 V. The electric field induced by this bias will tilt the potential profile shown on Fig. 1, but will not introduce any significant change in the values of the dipoles as will be shown in Section 4.

3. Operation of the gate

To a good approximation, the Hamiltonian of noninteracting quantum dots commutes with the Hamiltonian of the dipole–dipole interaction $\hat{V}_{int}$, which can be written as

$$\hat{V}_{\text{int}}|n, k\rangle = (-1)^{n+k+1}\hbar(J/2)|n, k\rangle, \tag{4}$$

where $\hbar$ is Plank's constant; $n = 0, 1$ denotes the state of the control qubit (the first dot); $k = 0, 1$ denotes the state of the target qubit (the second dot); and the constant of the dipole–dipole interaction is given by

$$\hbar J = \frac{p_c p_t}{2\pi\epsilon_0\epsilon_r R^3}, \tag{5}$$

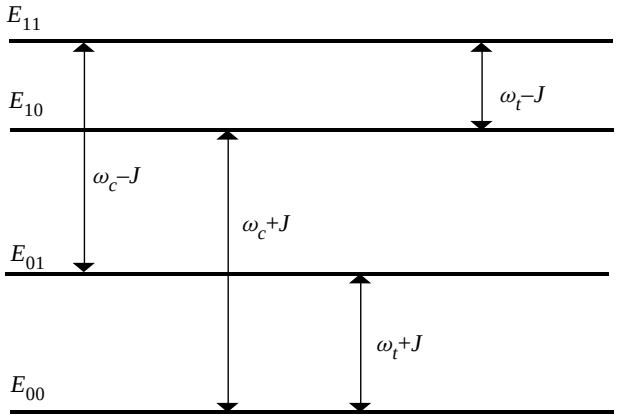

Fig. 2. Energy levels of two dipole–dipole interacting quantum dots. It is assumed that $|\omega_c| > |\omega_t|$.

where R is the distance between the dots, ϵ_0 and ϵ_r are the vacuum and relative dielectric permittivities, respectively. Throughout the paper, the subscripts c and t refer to the control and target qubits (or dots), respectively. One can see from eqns (4) and (5) that the system of interacting dipoles can be described by the Ising-type interaction where the dipoles associated with the confined quantum dot states act as *effective spins*. This particular form of the interaction Hamiltonian is desirable because all classical bit states are the eigenstates of this interaction, so that there is no undesirable time evolution of the quantum states. Meanwhile, application of an appropriate π pulse (or its fraction) to the target qubit can induce a time evolution which corresponds to the action of the XOR gate.

The overall Hamiltonian of the system is given by

$$\hat{H}(t) = \begin{pmatrix} -\frac{\hbar(\omega_c+\omega_t+J)}{2} & -\mu_t E(t) & -\mu_c E(t) & 0 \\ -\mu_t E(t) & \frac{\hbar(-\omega_c+\omega_t+J)}{2} & 0 & -\mu_c E(t) \\ -\mu_c E(t) & 0 & \frac{\hbar(\omega_c-\omega_t+J)}{2} & -\mu_t E(t) \\ 0 & -\mu_c E(t) & -\mu_t E(t) & \frac{\hbar(\omega_c+\omega_t-J)}{2} \end{pmatrix}. \tag{6}$$

Here $\mu_{c,t}$ is the dipole matrix element between states $|0\rangle$ and $|1\rangle$ in the control (target) qubit, and $E(t)$ is the optical field used to drive the gate. Using eqn (6) we can construct an energy diagram for two interacting dots in the absence of the field. This is shown in Fig. 2, where we have assumed that $\omega_c > \omega_t$. When the control dot is in state $|1\rangle$, the resonant frequency for the target dot becomes

$$\omega_t' = \frac{E_{11} - E_{10}}{\hbar} = \frac{1}{2}(\omega_c + \omega_t - J) - \frac{1}{2}(\omega_c - \omega_t + J) = \omega_t - J. \tag{7}$$

As a result, a π pulse of frequency $\omega_t - J$ causes the transition $|1\rangle \rightarrow |0\rangle$ only provided that the control dot is in state $|1\rangle$ (see Fig. 2). In order to be able to determine the state of the system experimentally, the coupling constant has to be relatively large so that

$$\Delta\omega \equiv \omega_{t,c} - J \leq \Gamma, \tag{8}$$

where Γ is the line broadening due to interaction with phonons, impurities, etc. The probability of spontaneous transitions has also to be small. The latter will be discussed in Section 5.

4. Calculation of dipoles and coupling constants

In order to determine the electron wavefunctions, confined energies, and dipoles for each quantum dot, we use the envelope function approximation. The three-dimensional confinement potential can be written as

$$U(x, y, z) = U_x(x)U_y(y)V(z), \tag{9}$$

where $V(z)$ is a finite quantum-well profile along the growth direction, and the $U_{x,y}$ are assumed to be infinite potential barriers in the normal plane. Neglecting excitonic effects, we may write the envelope function of a conduction band electron confined by the potential of eqn (9) as $\Psi = \phi(x)\psi(y)\chi(z)$, where $\phi(x),\ \psi(y)$ are regular particle-in-a-box states, and $\chi(z)$ is the envelope along the growth direction to be determined numerically. Since the confinement potential is modified along the z-direction, the relevant properties of the dot will be mostly defined by $\chi(z)$. This component of the wavefunction is found using the transfer matrix method [22] which allows us to take into account the potential profile variation and wavefunction barrier penetration. The dipoles due to the uneven charge distributions (see eqn (2)) in the c and t dots can now be rewritten as

$$p_{c,t} = \int_{-W_{c,t}/2-\Delta}^{W_{c,t}/2+\Delta} \chi_{c,t}(z) z \chi^*_{c,t}(z)\, dz. \tag{10}$$

Material parameters used in simulations correspond to GaAs. The electron effective mass is assumed to be $0.067m_0$, where m_0 is the free electron mass. The relative permittivity of GaAs is taken to be 10.9.

The charge density distributions for the first two confined states together with their corresponding confined energies, dipole moments and the profile of the confinement potential along the growth direction are shown in Fig. 3. The height of the potential step approximately corresponds to the heterojunction band offset between GaAs and $Al_{0.2}Ga_{0.8}As$. As one can see, the dipoles due to the uneven charge distributions along the growth direction are equal in absolute values but opposite in directions. The chosen potential profile gives a much better control of the equality $p_{\text{excited}} = -p_{\text{ground}}$ than the simple step well profile. It is interesting to note here that the dot size can be scaled up to a certain extent while keeping the ground state and the excited state dipoles equal in their absolute values. This is an important capability since (i) the resonance frequencies of the dots should be different: $\omega_c \neq \omega_t$; and (ii) this allows for the tuning of the dipole–dipole coupling constant J. One should note here, that it is almost impossible to meet the condition of eqn (3) for the simple symmetric dot (well) structure biased with an electric field. Fig. 4 shows such a structure biased with an $E = 50$ kV cm^{-1} electric field. As one can see, the dipoles due to the uneven charge distribution are very different in their values ($p_{\text{ground}} = -12$ e–Å and $p_{\text{excited}} = 1.5$ e–Å) so that the Ising-like interaction model is not applicable.

Using eqns (5) and (10), we have calculated the dipole–dipole interaction coupling constant for two asymmetric quantum dots with the potential profile shown in Fig. 3 (the lowest panel). The coupling constant J as a function of the effective size W of the dot is presented in Fig. 5. The solid curves correspond to the case when the size of both dots is scaled up, while the dashed curves corresponds to the case when the control dot size is fixed at 100 Å and only the target dot size is changed. The results are presented for several different dot separation distances. The curves denoted by letters A, B are plotted for dots grown on top of a substrate and are thus separated by air ($\epsilon_r = 1$). The dash-dotted curve C corresponds to two dots separated by a material with $\epsilon_r = 10.9$ when both dot sizes vary.

Rather large values of the coupling (as compared to the broadening) constant allow for experimental resolution of different quantum states. It also reduces the requirements for the π/N pulse selectivity. The length of the pulse τ_π has to be in the range specified by the condition below

$$\frac{1}{J} < \tau_\pi < \tau_{\text{coh}}, \tag{11}$$

where τ_{coh} is the quantum coherence time, which depends on the system structure and temperature. For the time allowed for computation (τ_{coh}), we want to use as many driving pulses as possible for increasing the

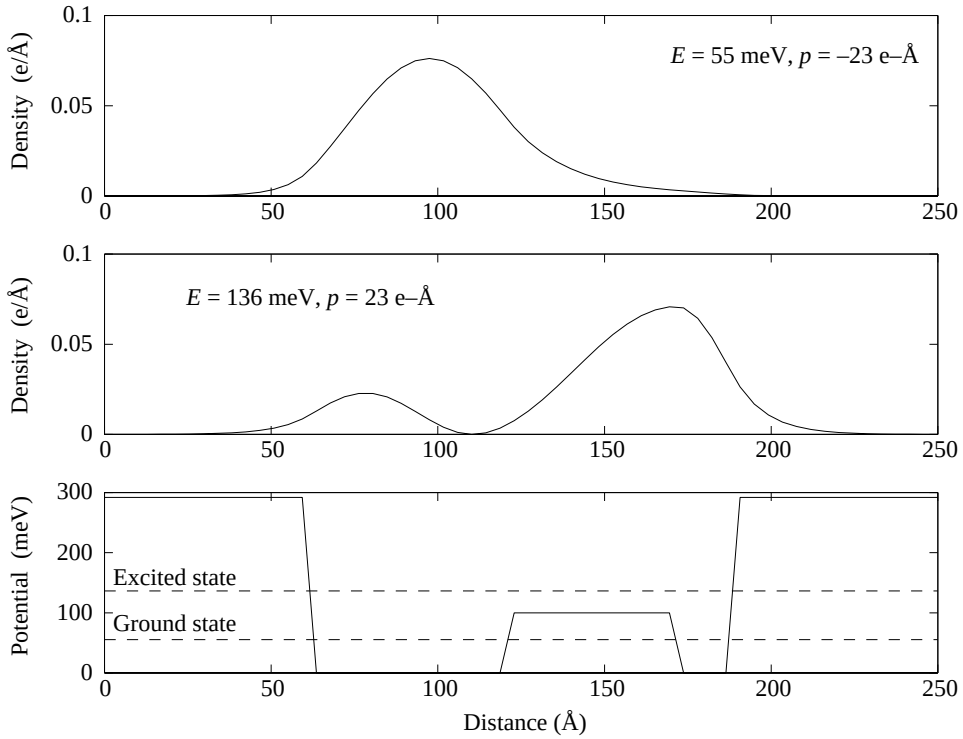

Fig. 3. Charge density distribution in the asymmetric quantum dot. Results are shown for the ground (upper panel) and first excited states (middle panel). Dipole moments due to the asymmetricity of the distributions are equal in absolute values but opposite in directions. A potential profile which creates such charge density distributions is shown below (lower panel).

number of computations. Since it is difficult to increase the upper limit of the inequality (11), we may try to decrease the lower limit. For the asymmetric dot implementation, the inverse of the coupling constant is on the order of 2.5×10^{-14} s. For comparison, the number obtained in Ref. [5] for the gate based on square potential quantum dots biased with an electric field is of the order of 10^{-12} s. This means that in our XOR gate driven with a femtosecond laser, it is possible to have a sufficient number of qubit manipulation steps. The only technological problem left here is the search for a femtosecond laser in the appropriate frequency range (intersubband transitions).

5. Quantum coherence requirements

It is well-known that a quantum computing algorithm can be implemented only if the quantum coherence of the system is preserved during the time of computation τ_{com}: $\tau_{\mathrm{com}} \leq \tau_{\mathrm{coh}}$. Here we estimate the limit of τ_{coh}, considering the dominant decoherence processes relevant to the proposed implementation. Under the assumption of having high quality structures at low temperatures, we may expect that the decoherence of our system occurs by spontaneous transitions between intersubband states which serve as the computational basis. These transitions include both radiative and non-radiative processes, which have been well studied for coupled asymmetric quantum well structures [23, 24]. In general, for quantum wells, the nonradiative lifetime of the transition ($|1\rangle \rightarrow |0\rangle$) is on the order of 0.1–10 ps while the radiative lifetime is on the order of 10–100 ns [23]. To our knowledge, the study of relaxation processes in quantum dots has not been completed. It remains a

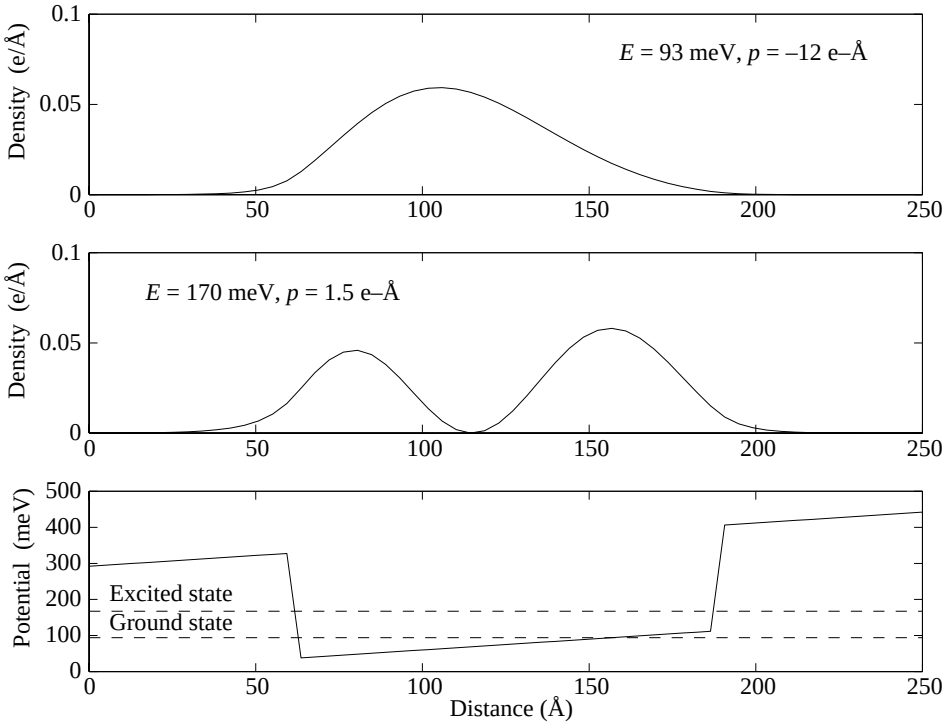

Fig. 4. Charge density distribution in the symmetric quantum dot biased with an electric field. Results are shown for the ground (upper panel) and first excited states (middle panel). Dipole moments induced by the electric field are very different in absolute values. A potential profile is shown below (lower panel).

subject of debate, particularly regarding the effect of the 'phonon bottleneck' on the carrier relaxation rates [25, 26]. It is generally believed, however, that the level quantization in quantum dots slows carrier relaxation toward the ground state and thus may increase the coherence time of our basic states.

Here, we evaluate the spontaneous radiative lifetime τ^r_{spon} and electron–phonon scattering time for a given geometry of our XOR gate structure. τ^r_{spon} can be found as [27]

$$\frac{1}{\tau^r_{\text{spon}}} = \frac{n_r e^2 E^2_{i,j}}{2\pi\epsilon_0 c^3 m_0 \hbar^2} f_{i,j}, \tag{12}$$

where n_r is the refractive index, c is the speed of light, $E_{i,j}$ is the intersubband separation energy between states i and j, and $f_{i,j}$ is the oscillator strength given by

$$f_{i,j} \equiv \frac{2m_0 E_{i,j}}{\hbar^2} |\langle j|z|i\rangle|^2. \tag{13}$$

We use eqns (11)–(13) to calculate τ^r_{spon} for transitions between the ground and the first excited states ($i = 0,\ j = 1$), and determine how it changes for different potential profiles. The results of the numerical simulations are presented in Table 1.

We can estimate the lifetime of the basic states limited by the non-radiative transitions using the formalism of Ref. [28]. It follows that phonon emission rate by an electron in the state i is given as

$$\frac{1}{\tau_{\text{ph}}} = \frac{2\pi}{\hbar} \sum_{f,q} \alpha^2(q) |\langle \Psi_f | e^{-iqr} | \Psi_i \rangle|^2 \delta(E_f - E_i + E_q)[N_0(T, E_q) + 1], \tag{14}$$

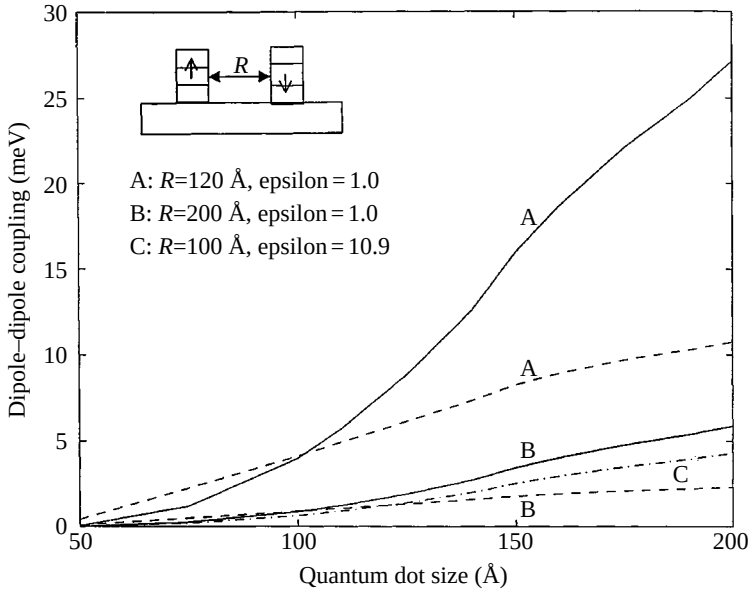

Fig. 5. Dipole–dipole coupling constant as a function of the dot size along the growth direction. The solid curves correspond to the case when the sizes of both dots are being scaled up. The dashed curves correspond to the case when the size of the control dot is fixed at 100 Å and only that of the target dot varies.

where the sum extends over all possible final-electron quantum numbers f and phonon wavevectors q, $N_0(T, E_q)$ is the Bose–Einstein distribution function, E_q is the energy of a phonon with wavevector q, T is the temperature, and α is the coupling constant. An analogous expression can be written for phonon absorption. One has to consider the coupling of electrons to longitudinal acoustic (LA) phonons via deformation potential and Fröhlich interaction between the electron and longitudinal optical (LO) phonons. These two mechanisms are expected to be dominant for our structure although much weaker than in the bulk. Interaction with longitudinal optical phonons in the quantum dot structure occurs when the level separation is close to the LO phonon energy $\hbar\omega_{LO}$. In our calculations we assume that $\hbar\omega_{LO} \approx 36$ meV. The expressions for the coupling constants are given in Ref. [28]. We perform the calculations with the material parameters which correspond to GaAs/AlGaAs system. The numerical simulation for $T = 4$ K shows that $\tau_{\rm ph} \approx 10^{-8}$–$10^{-7}$ for a 200 Å wide quantum dot structure, which is comparable to the radiative relaxation time. For higher temperatures, the non-radiative relaxation is stronger and $\tau_{\rm ph} < \tau^r_{\rm spon}$. Having these numbers in mind, let us assume that we use 100 fs laser pulse to drive our gate. Taking the average coupling constant from Fig. 5 and assuming that $\tau_{\rm coh} \approx 10^{-9} < \min\{\tau_{\rm ph}, \tau^r_{\rm spon}\}$, we can see that inequality eqns (11) holds: $10^{-14} < 10^{-13} < 10^{-9}$ for our gate. Thus, the strong coupling allows us to use fast laser pulses for optical driving of the quantum XOR gate and perform many computations during the time $\tau_{\rm coh}$ provided that the temperature is sufficiently low.

6. Conclusions

We propose an implementation of the quantum XOR gate based on *coupled asymmetric* quantum dots. The structure can be realized using state-of-the-art nanotechnology. The qubit preparation and manipulation is achieved by application of proper trains of π pulse fractions. The results of our numerical simulations show that the coupling constant of the dipole–dipole interaction in asymmetric dots can be tuned over a wide range by the choice of the potential profile, separation distances, and material parameters of the dots. This provides

Table 1: Spontaneous radiative lifetime vs. asymmetric dot size.

W, (Å)	τ^r_{spon} (s)
50	7.0×10^{-9}
100	5.0×10^{-8}
125	8.8×10^{-8}
150	1.2×10^{-7}
175	1.6×10^{-7}
200	1.8×10^{-7}

conditions for having the Ising-type interaction between the dots. The latter can be achieved more easily in our structure than in earlier proposed schemes based on symmetric quantum dots biased with an electric field. We also examine quantum coherence requirements for the operation of the quantum gate. Finally, we argue that our gate can be driven by a femtosecond laser if one is designed for an appropriate frequency range.

Acknowledgements—The work was partially supported by the Center for Integrated Space Microsystems, Jet Propulsion Laboratory (Dr B. Toomarian). The authors thank Dr F. Vatan and Professor V. P. Roychowdhury for discussions on quantum computing.

References

[1] J. I. Cirac and P. Zoller, Phys. Rev. Lett. **74**, 4091 (1995).
[2] N. A. Gershenfeld and I. Chuang, Science **275**, 350 (1997).
[3] G. J. Milburn, Phys. Rev. Lett. **62**, 2124 (1989).
[4] A. Shnirman, G. Schoen, and Z. Hermon, Phys. Rev. Lett. **79**, 2371 (1997).
[5] A. Barenco, D. Deutsch, A. Eker, and R. Jozsa, Phys. Rev. Lett. **74**, 4083 (1995).
[6] C. Monroe, D. M. Meekhof, B. E. King, W. M. Itano, and D. J. Wineland, Phys. Rev. Lett. **75**, 4714 (1995).
[7] J. A. Jones and M. Mosca, Implementation of a quantum algorithm to solve Deutsch's problem on a nuclear magnetic resonance quantum computer, LANL Preprint quant-ph/980127 (1998).
[8] W. G. Unruh, Phys. Rev. **A51**, 992 (1995).
[9] D. P. DiVincenzo, Topics in quantum computers, in *Mesoscopic Electron Transport*, Vol. 345 of NATO Advanced Study Institute, Series E: Applied Sciences, edited by L. Sohn, L. Kouwenhoven, and G. Schoen (Kluwer, Dordrecht, 1997) p. 657 (NATO Advanced Study Institute, Curacoa, 1996); preprint cond-mat/9612126.
[10] S. Bandyopadhyay, A. Balandin, F. Roychowdhury, and F. Vatan, Superlatt. Microstruct. **23**, 445 (1998).
[11] V. Roychowdhury, D. B. Janes, and S. Bandyopadhyay, Proc. IEEE **85**, 574 (1997).
[12] S. Bandyopadhyay, B. Das, and A. E. Miller, Nanotechnology **5**, 113 (1994).
[13] B. E. Kane, Nature **393**, 133 (1998).
[14] D. P. DiVincenzo, J. Appl. Phys. **81**, 4602 (1997).
[15] S. Lloyd, Science **261**, 1569 (1993).
[16] A. Balandin and K. L. Wang, in *Proceedings of the First NASA Int'l Conference on Quantum Computing and Quantum Communication, Feb, 1998, Palm Springs, CA*, edited by C. P. Williams, Springer-Verlag, Lecture Notes in Computer Science, (Springer-Verlag, Berlin, 1998) Vol. 1509.
[17] D. G. Austing, T. Honda, and S. Tarucha, Semicond. Sci. Technol., **11**, 388 (1996).
[18] S. Tarucha, D. G. Austing, and T. Honda, Superlatt. Microstruct. **18**, 121 (1995).

[19] S. Tarucha, D. G. Austing, T. Honda, R. J. van der Hage, and L. P. Kouwenhoven, Phys. Rev. Lett. **77**, 3613 (1996).
[20] R. Ashoori, J. Vac. Sci. Technol. **B15**, 2844 (1997).
[21] Y. J. Mii, R. P. G. Karunasiri, and K. L. Wang, Appl. Phys. Lett. **53**, 2050 (1988).
[22] P. F. Yuh and K. L. Wang, J. Appl. Phys. **65**, 4377 (1989); P. F. Yuh and K. L. Wang, Phys. Rev. **B38**, 8377 (1988).
[23] F. H. Julien, A. Sa'ar, J. Wang, and J.-P. Leburton, Electron. Lett. **31**, 838 (1995).
[24] S. I. Borenstain and J. Katz, Appl. Phys. Lett. **55**, 654 (1989).
[25] K. Mukai, N. Ohtsuka, H. Shoji, and M. Sugawara, Appl. Phys. Lett. **68**, 3013 (1996).
[26] S. Grosse, J. H. Sandmann, G. von Plessen, J. Feldmann, H. Lipsanen, M. Sopanen, J. Tulkki, and J. Ahopelto, Phys. Rev. **B55**, 4473 (1997).
[27] S. Datta, Quantum phenomena in *Modular Series on Solid State Devices* (Addison-Wesley, Reading, MA, 1989), Vol. II.
[28] U. Bockelmann and G. Bastard, Phys. Rev. **B42**, 8947 (1990).